Originally published as:

Parental magma of the Skaergaard intrusion: constraints from melt inclusions in primitive troctolite blocks and FG-1 dykes

Jakob K. Jakobsen · Christian Tegner · C. Kent Brooks ·
Adam J. R. Kent · Charles E. Lesher · Troels F. D. Nielsen ·
Michael Wiedenbeck

Abstract Troctolite blocks with compositions akin to the Hidden Zone are exposed in a tholeiitic dyke cutting across the Skaergaard intrusion, East Greenland. Plagioclase in these blocks contains finely crystallised melt inclusions that we have homogenised to constrain the parental magma to 47.4–49.0 wt.% SiO_2, 13.4–14.9 wt.% Al_2O_3 and 10.7–14.1 wt.% FeO^T. These compositions are lower in FeO^T and higher in SiO_2 than previous estimates and have distinct La/Sm_N and Dy/Yb_N ratios that link them to the lowermost volcanic succession (Milne Land Formation) of the regional East Greenland flood basalt province. New major- and trace element compositions for the FG-1 dyke swarm, previously taken to represent Skaergaard magmas, overlap with the entire range of the regional flood basalt succession and do not form a coherent suite of Skaergaard like melts. These dykes are therefore re-interpreted as feeder dykes throughout the main phase of flood basalt volcanism.

Keywords Skaergaard intrusion · Melt inclusions · Bulk composition · Parental magma · East Greenland

J. K. Jakobsen · C. Tegner
Department of Earth Sciences, University of Aarhus,
Høegh-Guldbergs Gade 2, 8000 Aarhus C, Denmark

J. K. Jakobsen (✉)
Nordic Volcanological Centre, Institute of Earth Sciences,
University of Iceland, Sturlugata 7, 101 Reykjavik, Iceland
e-mail: jakob@hi.is

C. K. Brooks
Geological Museum, Øster Voldgade 5-7,
1350 Copenhagen K, Denmark

A. J. R. Kent
Department of Geosciences, Oregon State University,
104 Wilkinson Hall, Corvallis, OR 97331, USA

C. E. Lesher
Department of Geology, University of California, Davis,
One Shields Avenue, Davis, CA 95616, USA

T. F. D. Nielsen
Geological Survey of Denmark and Greenland, Øster Voldgade
10, 1350 Copenhagen K, Denmark

M. Wiedenbeck
Helmholtz-Zentrum Potsdam Deutsches
GeoForschungsZentrum, Telegrafenberg C161,
14473 Potsdam, Germany

Introduction

The Eocene Skaergaard intrusion in East Greenland has been considered a type example of extreme fractional crystallisation of small basaltic magma chambers in the upper crust for almost 70 years (Irvine et al. 1998; McBirney 1995; Wager and Brown 1968; Wager and Deer 1939). A central problem for geochemical and petrological modelling of the Skaergaard intrusion is identification of the parental magma composition. This bears directly on important issues such as the liquid line of descent, the origin of the Pd–Au mineralisation hosted in the intrusion, volume estimates of exposed and unexposed parts of the intrusion, and the links between the intrusion and the contemporaneous flood basalt succession. Indeed, identification of parental magma compositions is a general problem for most plutonic rocks.

Previous estimates of the parent magma have been based on chilled samples from the margins of the intrusion (Hoover 1989a; Wager 1960), related dykes (Brooks

and Nielsen 1978, 1990) and mass-balance calculations (Ariskin 2002; Nielsen 2004). These methods all point to a ferro-tholeiitic composition. However, even small differences of less than a few wt.% SiO_2 or FeO, for example, may result in a huge variation in modelled magma compositions with prolonged fractional crystallisation (e.g. Bowen or Fenner trends). Melt inclusions provide alternative and direct information about the magma from which layered mafic intrusions crystallised (Li et al. 2005; Spandler et al. 2000, 2005). For Skaergaard, Hanghøj et al. (1995) showed that melt inclusions (now fully crystallised) represent an iron-rich ferrobasalt magma from which the Middle Zone crystallised. Furthermore, melt inclusions in apatite and olivine of the Upper Zone demonstrate that the evolved magma exsolved into iron- and silica-rich melts by silicate-silicate liquid immiscibility (Jakobsen et al. 2005).

Here we examine melt inclusions in plagioclase of primitive plagioclase-olivine (troctolite) cumulate rocks to evaluate the parental magma composition. An obstacle to this approach is that the most primitive cumulate rocks of the Skaergaard intrusion remain unexposed in the Hidden Series (McBirney 1996; Wager and Brown 1968). We therefore examine metre-sized blocks of primitive troctolite exposed in a ~15 m wide basaltic dyke cutting the intrusion (Irvine et al. 1998). We first describe the petrography, mineral chemistry, and whole rock composition of the troctolitic blocks and show that it is plausible that they originate from the unexposed part of the Skaergaard intrusion, as first speculated by Brooks and Nielsen (1990). We then describe the petrography and major and trace element composition of melt inclusions trapped in cumulus plagioclase of these troctolite blocks. We also re-examine the major and trace element composition of the related FG-1 dykes (Brooks and Nielsen 1978, 1990). The compositions of homogenised melt inclusions (47.4–49.0 wt.% SiO_2; 13.4–14.9 wt.% Al_2O_3; 10.7–14.1 wt.% FeO^T) are believed to represent a plausible magma composition. We discuss the merits of this composition relative to the FG-1 dykes and other suggested parental Skaergaard magmas and their petrogenetic links to the overlying flood basalt succession.

Geological setting

The ~55 Ma Skaergaard layered mafic intrusion measures approximately 11 × 7 km in outcrop (Fig. 1a) and is located at the mouth of the Kangerlussuaq fjord, East Greenland (Brooks and Gleadow 1977; Gleadow and Brooks 1979; Hirschmann et al. 1997; Hamilton and

Brooks 2004). The emplacement of the intrusion is intimately linked to an episode of crustal extension, rifted margin formation and outpourings of a 6–10-km thick flood basalt succession during the opening of the Northeast Atlantic (Andreasen et al. 2004; Irvine et al. 1998; Tegner et al. 1998a). The box-shaped intrusion was emplaced at the unconformity between the Archean basement and the overlying flood basalts and was accommodated by steep boundary faults (Irvine 1991; Nielsen 2004). Pressure estimates demonstrate that the intrusion was emplaced into a thin volcanic cover, at a depth equivalent to a pressure of 0.7 ± 0.5 kbar at the roof contact, but subsided during crystallisation, due to emplacement of flood basalts over the intrusion, to a depth equivalent to 3.0 ± 1.3 kbar at the roof contact (Larsen and Tegner 2006).

Traditionally, the intrusion is divided into: (a) the Layered Series (LS), which is the most prominent unit and crystallised upwards from the bottom of the magma chamber; (b) the Upper Border Series (UBS) that solidified from the top and downwards; and (c) the Marginal Border Series (MBS) that crystallised inwards from the walls (Naslund 1984; Wager and Brown 1968; Wager and Deer 1939). Each of these units is subdivided into zones and subzones based on their cumulus mineralogy (see McBirney 1996 and references therein). The intrusion has undergone extreme fractionation which is clearly reflected in the composition of the latest cumulates with six cumulus phases and pure iron end-members for pyroxene (hedenbergite) and olivine (fayalite) and sodium-rich plagioclase. The UBS and the LS meet at the Sandwich Horizon, which is generally believed to represent the final liquid (McBirney 1996; Wager and Brown 1968).

The lowest part of the LS is unexposed and is traditionally referred to as the Hidden Zone (HZ), its relative size is unknown but various estimates for HZ range from 15 to 70% of the entire intrusion (Blank and Gettings 1973; Maaløe 1976; Norton et al. 1984; Wager 1960). The lowermost part of LS denoted Lower Zone a (LZa) and the drilled part of HZ have essentially the same mineralogy (Maaløe 1976) and consist of cumulus plagioclase and olivine with poikilitic augite. Inverted pigeonite and interstitial oxides occur in small amounts. The MBS pertinent for this contribution forms the eastern and western side of the intrusion (Fig. 1a) and ranges from 70 to 600 m in width (Hoover 1989b). Wager and Brown (1968) divided the MBS into an outer 'tranquil division' and an inner 'banded division'. The outer edge of the tranquil division is in places highly variable in compositions and appears to represent pulses of magma (Holness et al. 2007; Hoover 1989b).
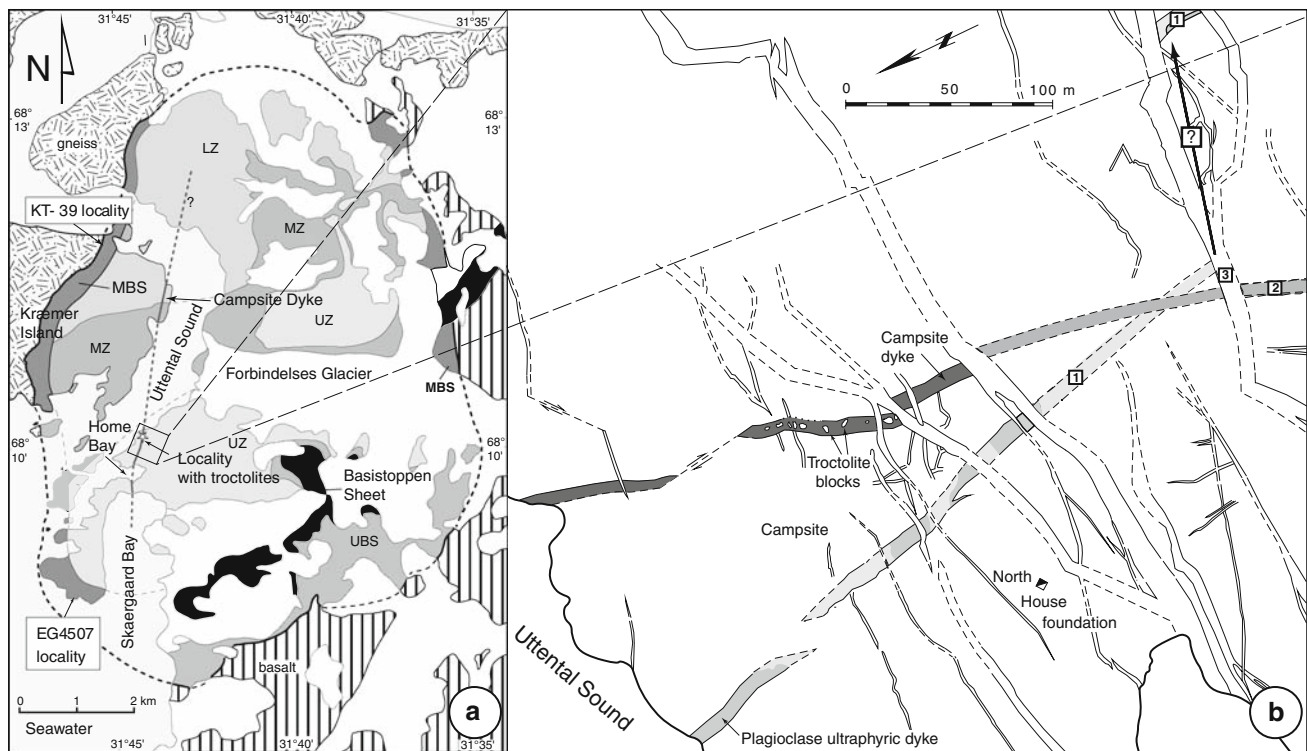
Fig. 1 Location and map of the Campsite Dyke. **a** Map of the Skaergaard intrusion with the Campsite Dyke marked with a grey line. Sample locations for chilled margins discussed in the text are shown; EG4507 (Wager 1960) and KT-39 (Hoover 1989a). FG-1 dykes are 10 km off the map to the west. *MBS* Marginal Border Series, *UBS* Upper Border Series, Layered Series Zones: *LZ* Lower Zone, *MZ* Middle Zone. *UZ* Upper Zone. **b** Close-up of Homestead

area (inset on Fig. 1a) showing the complex array of dykes, their cutting relations and location of the studied troctolite blocks. *Dashed line/lighter shading* indicates that the dykes are not well exposed. *Square boxes* with *numbers* refer to the inferred relative ages of the dykes (Irvine et al. 1998). Notice that this map is rotated compared to the map **a**. Map **b** is modified from Irvine et al. (1998)

Field relations and petrography

Dykes in the Home Bay area

The dykes in the study area (Fig. 1), first described by Vincent (1953), cut the Upper Zone cumulates and have compositions ranging from dolerite to camptonite. The structurally youngest dykes trend East–West (Fig. 1b) and are greenish grey, with mildly alkaline composition and belong to a much younger regional dyke swarm (Irvine et al. 1998; Nielsen 1978) and are not of interest to this study. The structurally oldest, North–South trending dyke (number 1 in Fig. 1) is laden with tabular plagioclase phenocrysts up to 3 cm long and chilled against the Skaergaard host gabbro. The groundmass consists of augite, olivine, oxides and greenish altered mesostasis. The plagioclase laths are partly sericitised and contain numerous melt inclusions. Irvine et al. (1998) referred to this dyke as 'plagioclase porphyry' but we refer to it as 'plagioclase ultraphyric'. To our knowledge, it is unique in the area.

The dyke labelled 2 in Fig. 1 carries metre-sized blocks of troctolite described below. This occurrence was first

mentioned by Brooks and Nielsen (1990) and described in some detail by Irvine et al. (1998). The dyke is prominently exposed close to the remains of the most northerly of the expedition houses used by L. R. Wager and Irvine et al. (1998) named it the 'Campsite composite basaltic dyke' but for brevity we refer to it as the 'Campsite Dyke'. The Campsite Dyke weathers brown, is ~15 m wide, is almost vertical, trends approximately north-south, and can be followed for over ~1,200 m in the study area from the Skaergaard Bay to Uttental Sund (Fig. 1a). The full length of the dyke is uncertain. However, on Kraemer Island, about two kilometres farther north and across Uttental Sund, there is a virtually identical brown-weathering, North–South trending dyke that according to Irvine et al. (1998) appears to be an extension of the Campsite Dyke. Both the Campsite Dyke and the plagioclase ultraphyric dyke are structurally old, with the ultraphyric dyke interpreted as being the oldest (Irvine et al. 1998). The Campsite Dyke is composite with an outer member that is about 15 to 70 cm wide on each side, chilled against the host gabbros, and devoid of blocks (Fig. 2). The central member is typically >10 m wide and chilled against the outer member. The chill of the outer
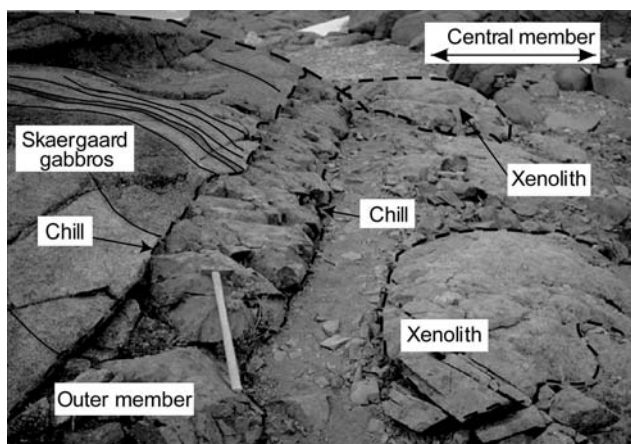
Fig. 2 Photograph of the Campsite Dyke showing the inner central member with metre-size coarse-grained blocks, the outer member and the layered Skaergaard Upper Zone cumulates that are cross-cut by the dyke. Hammer for scale

member contain phenocrysts of plagioclase (2–3 mm), sometimes as glomeroporphyritic aggregates composed of 10–20 individuals, olivine (1–2 mm) and sparse mm-sized clinopyroxene phenocrysts (Fig. 3). Inwards, the grain size of the central member increases and the texture changes to subophitic and porphyritic with plagioclase laths up to 1 cm long (Fig. 3). The central member is locally crowded with metre-sized blocks of troctolite blocks described below.

Blocks of troctolite in the Campsite Dyke

A ~100 m long end segment of the Campsite Dyke (Fig. 1) contains about 40 blocks ranging in size from a few centimeters to 3 m across (Fig. 2). Several types of blocks are present, but the most prominent are troctolitic although there are also olivine gabbros, some small, brown-weathering basalts and a few sedimentary xenoliths (Irvine et al. 1998). The fine-grained basaltic blocks are explained as cognate pieces of the marginal zones of the Campsite Dyke (Irvine et al. 1998).

The plutonic blocks in the Campsite Dyke divide into three compositionally and texturally different types (Irvine et al. 1998): (1) gabbroic troctolite; (2) laminated troctolite; and (3) olivine gabbro. We here describe the most abundant blocks in the Campsite Dyke. They correspond to the gabbroic troctolite of Irvine et al. (1998). The troctolites are poikilitic rocks in which plagioclase laths up to 2 cm constitute the main cumulus phase. Cumulus olivine, 1–2 mm in size, is also present together with poikilitic augite oikocrysts and sparse intercumulus Fe–Ti oxides (Fig. 3a).

Skaergaard-related FG-1 dykes

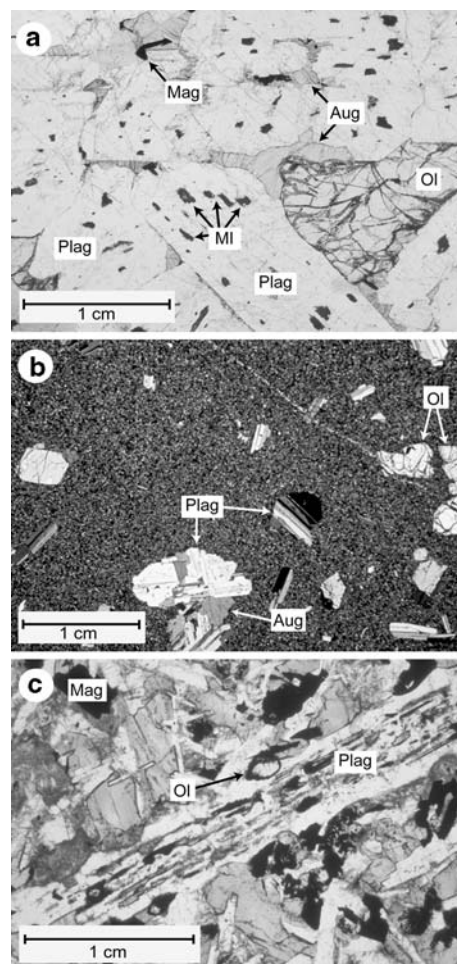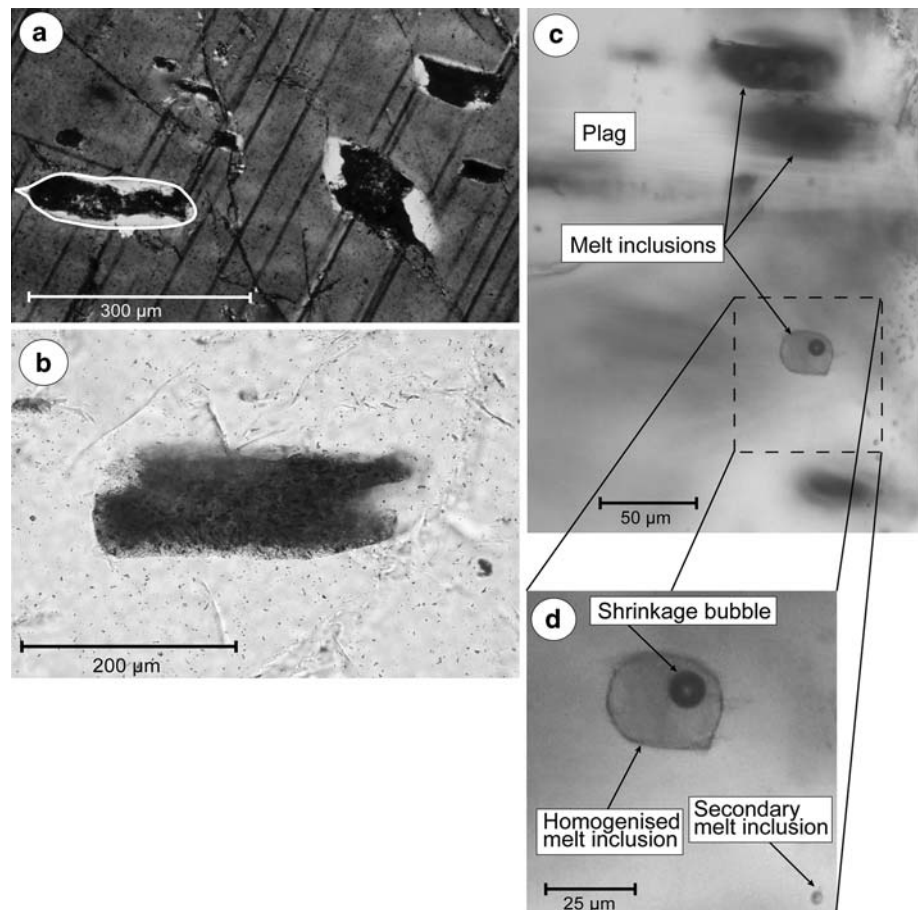The magma compositions represented by the FG-1 dyke swarm, located on Kraemer Island ~10 km west of the

Fig. 3 Microphotographs of dyke rocks and troctolite blocks. **a** Troctolite block with poikilitic texture, abundant melt inclusions and crystal inclusions. Some melt inclusions (MI) are shown with *arrows*. **b** Chill of outer member of the Campsite Dyke with olivine, plagioclase and augite phenocrysts. (Crossed nicols.) **c** Plagioclase ultraphyric dyke with large plagioclase laths in the central part of the picture

Skaergaard intrusion (not shown in Fig. 1), and on Uttental Plateau just north of the intrusion, have been interpreted as equivalents to the parental and evolved magmas of the intrusion (Brooks and Nielsen 1978, 1990) and have been used experimentally for modelling the evolution of the Skaergaard magma (Thy et al. 2006; Toplis and Carroll 1995). Five compositional groups, labelled A to E in order of decreasing Mg#, have been identified. The FG-1 dykes are typically 8–14 m wide and are doleritic in texture with fine grained chilled margins. Brooks and Nielsen (1978) presented major and some trace elements for samples of the central portion of five dykes. Later, Brooks and Nielsen (1990) presented major element compositions for four marginal samples and demonstrated that the compositions of marginal and central samples of individual dykes in most only deviate marginally from the compositions of the

Fig. 4 Microphotographs of melt inclusions in plagioclase. **a** Melt inclusions from the troctolitic blocks in the Campsite Dyke. Notice light coloured (albitic) rim around the inclusions. The true outline of the melt inclusion on the left is marked by a white line. (Crossed nicols.) **b** Close-up of a single melt inclusion showing microcrystalline texture. **c** Reheated melt inclusions in plagioclase (mounted in epoxy) from the troctolite blocks in the Campsite Dyke. Several other melt inclusions are visible but not in focus due to their subsurface location. **d** Blow-up of **c** showing reheated melt inclusion with shrinkage bubble and a single secondary melt inclusion

Melt inclusions in plagioclase

Figure 4 illustrates microcrystalline melt inclusions in plagioclase from the troctolite blocks. The melt inclusions are characterised by rims of sodic plagioclase formed as a result of host crystallisation on the walls of the inclusion (Fig. 4a). The inclusions are up to 400 μm in diameter (including the area that have suffered post-entrapment crystallisation), are microcrystalline and are some times altered. The non-plagioclase parts of the inclusions often have an angular, corrugated outline, whereas the whole inclusion itself is more rounded (Fig. 4a). Small anhedral oxide daughter minerals occur in the inclusions, pyroxene and other silicate phases are also recognised but are generally too small to identify unequivocally (Fig. 4b). The presence of microcrystalline to glassy melt inclusions in blocks of coarse grained

centres of the dykes. This implies that both the marginal and the central samples represent approximations to magma compositions. We present new major- and trace element data for eight additional dykes representing types FG-1 A, B, C and E.

troctolite is surprising, as the slow cooling rate implied by their texture would normally result in fully crystallised melt inclusions similar to those described in the LS (Hanghøj et al. 1995). We tentatively explain the glassy nature of the melt inclusions as a result of natural reheating and rapid cooling of the dyke (I. V. Veksler, personal communication 2003).

Analytical methods

Whole rock data were obtained by jaw crushing (steel) of the samples followed by grinding in a Tungsten-Carbide shatterbox. The samples were analysed by X-ray fluorescence (XRF) at the Department of Earth Sciences, University of Aarhus, using a Philips PW 2400 instrument. Major elements, except FeO, were determined using fused glass pellets consisting of flux (66% $Li_2B_4O_7$ and 33% $LiBO_2$) and crushed sample in the ratio 1:5. FeO was determined by titration with dichromate and all Mn_3O_4 has been recalculated to MnO. The FG-1 dyke samples were analysed by XRF at the Geological Institute, University of Copenhagen, following the procedure described by Kystol and Larsen (1989).

For our melt inclusion studies, samples were crushed and plagioclase crystals were separated by sieving and hand-picking, washed in water and finally by ethanol. Heating experiments were conducted in a vertical furnace and the temperature was calibrated to the melting point of gold (1,064°C) within ±5°C. The samples were not heated under controlled oxygen fugacity but instead kept in a reducing atmosphere by adding graphite powder to prevent oxidisation. The samples were held for approximately 30 min at the chosen temperature and were then quenched in air. Heating experiments using 10°C increments demonstrated that total homogenisation of melt inclusions in plagioclase from troctolite blocks takes place at 1,185°C. This is based on optical examination of melt inclusions (in microscope) and BSE images showing complete dissolution of daughter phases and no sodic rims in the surrounding plagioclase which is also confirmed by EMP line scans showing that the host plagioclases were homogenous on each side of the melt inclusions. The reheated melt inclusions (Fig. 4c) typically have shrinkage bubbles (Fig. 4d) making up a constant volume of 5–10% that nucleate during isochoric (constant volume) cooling of a trapped homogeneous liquid. Reheating does not necessarily imply disappearance of the bubble (Frezzotti 2001; Sobolev and Shimizu 1993). In order to minimise the risk of overheating the inclusions (see below) we avoided homogenising them to the point where the shrinkage bubble disappears (Danyushevsky et al. 2002). We do not believe that this is a problem, as we have not attempted to determine the volatile contents in the melt inclusions. Some inclusions typically >150 μm ones had large bubbles, and crystallised euhedral magnetite crystals during heating experiments. These inclusions are interpreted as altered hydrated inclusions, and were discarded for analyses. Following heating the host crystals were mounted in epoxy, ground with carbide adhesive paper to expose inclusions, and finally polished with diamond- or alumina powder. Exposed melt inclusions were examined and documented using transmitted and reflected light and with electron back-scattered images.

Melt inclusions and minerals were analysed by electron microprobe for major elements. The analyses were preformed at the Geological Institute, University of Copenhagen, on a JEOL 8000 Superprobe and at the Department of Earth Sciences, University of Aarhus, using a JEOL JXA-8600 Superprobe with four wavelength-dispersive spectrometers (WDS) and one energy-dispersive spectrometer (EDS). The microprobe was operated at either a beam current of 10 nA for analysis of melt inclusions or 15 nA for mineral analyses, using a 15 kV accelerating voltage. To minimize the loss of Na, a defocused beam of 20 μm was used to analyse melt inclusions and plagioclase. Only melt inclusions free of cracks in the surrounding plagioclase and having a diameter of <100 μm were analysed. Each inclusion was analysed two to four times to check homogeneity. Olivine and pyroxene were analysed using beam sizes of 5 and 2 μm, respectively.

Trace elements in homogenised melt inclusions from CKB 89-13 were analyzed by secondary ion mass spectroscopy (SIMS) at Helmholtz-Zentrum Potsdam, Deutsches GeoForschungsZentrum, using a Cameca 6f ion microprobe. Analyses followed techniques outlined in Kent and Elliott (2002) and Kent et al. (2002). Analyses were obtained using a 5–20 nA primary O^- beam focused to 15–30 μm, and during analysis a field aperture with effective field of view of ~ 30 μm was centered over the point to be analysed. Observed ionic counts were normalised to ^{42}Ca, and the absolute concentrations of trace elements were calculated on the basis of CaO measured by electron microprobe relative to normalised values measured in NIST 610 and BSR-2G reference glasses. Interference of LREE, MREE and Ba oxides on MREE and HREE were corrected for by peak stripping, with the magnitude of interferences calculated using oxide production factors measured in synthetic glasses. A glass made from BIR-1 rock powder was also analysed in order to assess accuracy. Measured values show good agreement (typically within ±10%) with the accepted values. In general, we estimate the following analytical uncertainty at 2 s: $\leq \pm 5\%$ for Ce and Dy; $\leq 10\%$ for La, Nd, and Eu; $\leq 15\%$ for Sm, Gd, and Yb and <20% for Er.

Rare earth element compositions of the dykes and troctolite blocks were determined using an Agilent Technologies 7500a Quadrupole ICPMS at the University of California, Davis, USA. Samples of 100 mg were dissolved in 10 ml of 2:1 distilled concentrated HF and HNO_3 in sealed Teflon beakers. Samples were heated at 150°C and put into ultrasonic bath to promote dissolution of grains. When in solution the samples were dried down to a gel on a hot plate. Finally the dissolved samples were added to 80 ml of 3% HNO_3 and the internal standard. The solution ICPMS analyses were calibrated against BIR-1, BHVO-2 and W2 prepared identically to the unknowns.

Results

Whole rock compositions of troctolite blocks and host dykes

Table 1 presents whole rock compositions of the Campsite Dyke, where we have sampled the central member and a chill from the outer member, the plagioclase ultraphyric dyke and the troctolite blocks. The Campsite Dyke is a ferrobasalt with 47–48 wt.% SiO_2, Mg# (100 × Mg/ Mg + Fe^{2+}) 49 and normative plagioclase An-content

Table 1 Major- and trace elements of Campsite Dyke, plagioclase ultraphyric dyke and troctolite blocks

Sample #	Campsite Dyke		Plagioclase ultraphyric dyke		Troctolite blocks	
	Chill CKB03-1	Central CKB84-406	Chill CKB03-2	Central CKB03-3	CKB03-4	CKB89-13
SiO_2	47.08	47.95	45.98	47.48	47.60	47.22
TiO_2	2.15	2.35	3.23	3.23	0.67	0.64
Al_2O_3	14.94	14.82	12.90	15.23	22.21	22.48
Fe_2O_3	3.44	3.73	2.33	2.87	1.62	1.04
FeO	8.20	8.46	10.14	8.45	3.97	4.38
MgO	7.56	6.46	7.60	6.32	6.51	6.72
MnO	0.19	0.24	0.20	0.180	0.10	0.09
CaO	12.47	11.66	11.12	11.12	14.81	14.71
Na_2O	2.24	2.34	2.90	2.90	1.73	1.76
K_2O	0.33	0.37	0.33	0.57	0.11	0.10
P_2O_5	0.21	0.24	0.38	0.36	0.05	0.05
LOI	1.36	1.61	2.60	1.21	0.90	0.97
Sum	100.17	100.23	99.71	99.92	100.28	100.16
FeO^T	11.30	11.82	12.24	11.03	5.43	5.32
Mg#	54.4	49.3	52.5	50.5	68.1	69.3
CIPW weight norm						
Or	1.95	2.23	1.89	3.43	0.65	0.59
Ab	19.75	20.12	25.30	24.93	14.69	14.83
An	29.60	29.31	21.81	27.19	52.92	53.21
Di	25.49	22.99	26.45	21.48	16.73	15.7
Hy	5.36	13.33	0.13	4.8	4.92	2.9
Ol	10.43	4.62	14.06	8.39	7.38	9.35
Mt	2.77	2.3	3.04	2.71	1.32	1.29
Il	4.14	4.53	6.32	6.23	1.27	1.22
Ap	0.49	0.57	0.9	0.86	0.12	0.12
Norm An%	59.7	59.3	44.9	50.8	77.2	77.1
V	313	306	324	300	139	125
Sr	427	428	454	496	412	429
Y	21.4	26.0	28.1	27.0	7.69	8.21
Zr	139	270	205	215	33	35
Nb	16.1	31.1	33.1	32.1	3.25	3.31
Ba	88	129	155	126	38.2	37.4
La	15.26	25.12	26.20	25.68	3.08	3.01
Ce	37.82	59.00	61.50	59.98	7.54	7.48
Pr	5.45	8.16	8.57	8.37	1.08	1.12
Nd	23.80	34.03	35.70	34.74	5.52	5.51
Sm	5.57	7.54	7.89	7.67	1.43	1.41
Eu	1.82	2.42	2.35	2.39	0.75	0.84
Gd	5.22	6.68	7.00	6.77	1.97	2.03
Tb	0.79	0.99	1.04	1.00	0.28	0.25
Dy	4.32	5.43	5.74	5.55	1.30	1.28
Ho	0.80	0.99	1.06	1.02	0.26	0.33
Er	2.02	2.43	2.61	2.51	0.71	0.75
Tm	0.28	0.33	0.36	0.35	0.10	0.13
Yb	1.62	1.94	2.14	2.03	0.42	0.39
Lu	0.23	0.27	0.29	0.28	0.08	0.09

All oxides in weight %; *LOI* loss on ignition. Trace elements in µg/g. Mg# = $100 \times$ Mg/(Mg + Fe), An% = $100 \times$ Ca/(Ca + Na)

[100 × Ca/(Ca + Na)] 59. There is only a slight chemical difference between the chilled outer member and the central member of the Campsite Dyke. The chill from the outer member is slightly more primitive (Mg# 54), richer in Al_2O_3, CaO and MgO and lower in TiO_2, Na_2O and K_2O (Table 1). The plagioclase ultraphyric dyke also has a ferrobasaltic composition but is higher in P_2O_5, TiO_2, K_2O, Na_2O and has a more sodic plagioclase composition than the Campsite Dyke. The chilled margin of the plagioclase ultraphyric dyke has lower SiO_2 and Al_2O_3 and higher MgO and FeO than the central member of the Campsite Dyke.

The high Al_2O_3 (~22 wt.%), and the low content of excluded components such as K_2O, TiO_2 and P_2O_5 in the troctolite (Table 1) confirm the plagioclase-rich nature of the blocks. These are all features to be expected in such cumulate rocks. The troctolite blocks are the most primitive of the analysed specimens with Mg# 68–69 and a normative plagioclase composition of An_{77}, and they are also more primitive than the most primitive cumulates known in the Skaergaard intrusion (<An_{68} and bulk Mg# <60 McBirney 1989, 1996; Wager and Brown 1968). Compositions are rather variable but resemble the calculated cumulate extract of Brooks and Nielsen (1978) for the first stage in the evolution of the Skaergaard-type liquids (Brooks and Nielsen 1978; Table 4), except that MgO is higher and the normative plagioclase slightly lower in the calculated composition. Primitive mantle normalised concentrations for dyke compositions, shown in Fig. 5a, define a coherent group for the two samples from the plagioclase ultraphyric dyke and the central member of the Campsite Dyke whereas the chill from the Campsite Dyke is characterised by a more flat trace element pattern and lower concentrations. The troctolite blocks have, in contrast to the dyke samples, a strong positive Sr anomaly and Eu peak due to the high plagioclase content but otherwise are depleted in trace elements compared to the analysed dyke rocks (Fig. 5a).

Whole-rock compositions of FG-1 dykes

Major and trace element compositions of the FG-1 dykes are given in Table 2. All the dykes are evolved ferrobasalts. Dykes A, B and C form a group with high SiO_2 (47–48 wt.%), high Mg# (54.4–51.3), and low TiO_2 (2–3 wt.%) relative to dyke E with SiO_2 between 45 and 46 wt.%, Mg# 39.5–43.0 and about 5 wt.% TiO_2. All the FG-1 samples analysed are hypersthene normative and half of them are quartz normative, the other half being olivine normative. Compared to the previously published data by Brooks and Nielsen (1978, 1990) and Thy et al. (2006), the new data vary only slightly. Composition for the type C dyke is quite similar to the Kramer Island macrodyke (Momme and Wilson 2002). Trace element compositions for FG-1 dykes
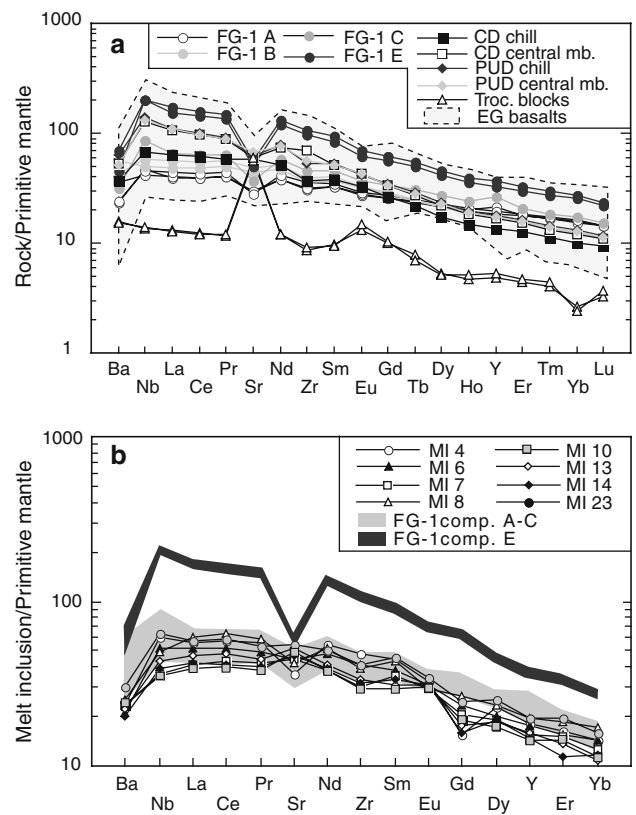

Fig. 5 Primitive mantle normalised (McDonough and Sun 1995) trace element abundance patterns for analysed dykes, troctolite blocks and the melt inclusions. **a** Composition of plagioclase ultraphyric-, Campsite- and FG-1 dykes. The East Greenland Plateau Basalts (Andreasen et al. 2004; Peate and Stecher 2003; Tegner et al. 1998b) are shown as shaded area for comparison. **b** Melt inclusions from troctolite blocks in the Campsite Dyke. *Light shaded area* is FG-1 dykes composition A–C and *dark shaded area* is FG-1 composition E

(Table 2) have LREE-enriched chondrite normalised patterns with La/Sm$_N$ = 1.3–1.9, plot in the broad field representing the High-Ti Series of the East Greenland Plateau Lavas (Fig. 5a) (Larsen et al. 1989; Tegner et al. 1998b), and are more LREE-enriched, compared to the previous results of Brooks and Nielsen (1978) on the dyke suite.

Mineral compositions of phenocrysts and troctolite blocks

The plagioclase composition in the troctolite blocks ranges from An_{79} to An_{82}, similar to phenocrysts in the outer member of Campsite Dyke (An_{80}; Table 3). The cores of plagioclase phenocrysts in the central member of Campsite Dyke and the plagioclase ultraphyric dyke have An_{74} to An_{76}. Zoned rims of plagioclase phenocrysts range down to An_{56} for the plagioclase ultraphyric dyke and An_{44} for Campsite Dyke. Interstitial matrix plagioclases range down to An_{31} in the plagioclase porphyry dyke and An_{42} in the Campsite Dyke.

Table 2 Major- and rare earth elements concentrations in FG-1 dykes

Dyke	A	A	A	B	B	C	E	E
Sample	40,537	361,042	361,043	361,034	361,037	40,536	361,045	361,046
SiO_2	48.02	48.01	47.87	46.69	47.88	48.25	45.47	46.10
TiO_2	2.14	2.16	2.15	2.58	2.33	2.93	5.33	4.80
Al_2O_3	13.80	14.41	14.45	14.62	14.91	13.34	12.05	12.71
Fe_2O_3	1.72	2.20	1.17	1.81	1.94	1.93	3.41	3.55
FeO	10.90	10.22	10.46	10.11	10.27	11.95	13.14	12.65
MnO	0.19	0.20	0.19	0.20	0.20	0.20	0.24	0.23
MgO	7.15	6.81	6.99	5.97	6.16	6.31	5.55	4.63
CaO	11.38	11.18	11.33	11.28	11.17	10.70	9.63	9.32
Na_2O	2.30	2.10	2.19	2.29	2.22	2.46	1.66	2.79
K_2O	0.31	0.33	0.26	0.40	0.37	0.45	0.38	0.61
P_2O_5	0.20	0.19	0.21	0.24	0.22	0.29	0.65	0.70
LOI	1.19	1.39	1.46	1.59	1.74	1.29	1.59	1.18
Sum	99.29	99.21	98.73	97.76	99.41	100.10	99.10	99.25
FeO^T	12.45	12.20	11.51	11.74	12.01	13.69	16.21	15.84
Mg#	53.9	54.3	54.4	51.3	51.7	48.5	43.0	39.5
CIPW weight norm								
Qz		0.14			0.05		5.69	1.46
Or	1.89	2.01	1.6	2.48	2.25	2.72	2.3	3.66
Ab	19.8	18.19	19.04	20.14	19.21	21.07	14.38	24.03
An	26.94	29.54	29.65	29.55	30.35	24.3	24.94	20.78
Di	24.12	21.3	21.99	22.26	20.52	22.79	16.26	18.02
Hy	14.94	20.91	17.84	14.4	19.67	18.04	19.43	15.85
Ol	5.16		3.45	2.79		1.94		
Mt	2.54	3.26	1.74	2.73	2.89	2.83	5.07	5.25
Il	4.14	4.2	4.2	5.09	4.54	5.64	10.39	9.29
Ap	0.46	0.44	0.51	0.58	0.53	0.67	1.55	1.65
Norm An%	56.19	60.48	59.48	58.04	59.83	52.11	62.04	44.91
V	440	379	329	392	381	483	428	332
Sr	211	217	206	355	317	269	359	406
Y	33.95	29	31	27	28	41.31	52	58
Zr	118	123	136	150	138	172	370	403
Nb	11.3	10.1	11.0	14.1	12.2	20.4	48.0	49.2
Ba	56	85	59	103	137	76	109	167
La	9.40	9.55	10.39	13.20	11.65	15.42	36.06	40.45
Ce	24.02	24.24	26.36	33.86	29.80	38.65	87.20	97.69
Pr	3.77	3.80	4.09	5.19	4.62	5.85	12.45	13.86
Nd	17.48	17.59	18.91	23.72	21.29	26.42	54.44	60.80
Sm	4.84	4.82	5.08	6.02	5.51	6.83	12.56	13.82
Eu	1.55	1.56	1.62	1.82	1.76	2.08	3.49	3.92
Gd	5.17	5.16	5.41	5.79	5.52	6.76	11.26	12.47
Tb	0.86	0.85	0.90	0.90	0.88	1.11	1.78	1.96
Dy	5.33	5.33	5.63	5.30	5.26	6.68	10.25	11.28
Ho	1.09	1.08	1.14	1.01	1.03	1.31	1.98	2.17
Er	2.84	2.85	2.97	2.52	2.59	3.29	4.84	5.22
Tm	0.41	0.41	0.43	0.34	0.35	0.46	0.68	0.73
Yb	2.51	2.50	2.63	1.98	2.07	2.78	4.11	4.33
Lu	0.35	0.35	0.36	0.27	0.28	0.38	0.55	0.57

Major elements in weight %. All trace elements in μg/g. *LOI* loss on ignition

Mg# = 100 × Mg/(Mg + Fe), normative An% = 100 × Ca/(Ca + Na)

The micro phenocrysts of olivine in the chilled margin of the Campsite Dyke have compositions of Fo_{78-81} and the troctolite blocks have Fo_{77-78}; phenocrysts from the chill are only slightly more primitive than olivine from the troctolite blocks (Fo_{79-82}). The pyroxenes in the Campsite Dyke have Mg# 77, which is a little more evolved than the sparse pyroxene phenocrysts in the chill of the outer member of the dyke (Mg# 80–81; Table 3). The blocks in the troctolite have clinopyroxene Mg# 81 and the ultra-phyric dyke clinopyroxene Mg# $\sim$75.

Composition of homogenised melt inclusions

Major- and trace element compositions for the homogenised melt inclusions are given in Table 4. All inclusions have ferrobasaltic compositions with 47–49 wt.% SiO_2, 11–14 wt.% FeO^T and Mg# 47–53. Analysed melt inclusions show some variations in major element compositions particularly for CaO (11.4–14 wt.%), Na_2O (2.23–4.66 wt.%) and K_2O (0.21–0.66 wt.%) whereas elements like Si, Mg Al and Ti vary relatively little. Trace elements for the melt inclusions define a coherent group partly overlapping with the FG-1 A-C compositions but have steeper trace element patterns from Sm to Gd and slighter flatter pattern from Gd to Yb (Fig. 5b). The melt inclusions are characterised by a weak positive Eu anomaly and quite variable Sr concentrations, chondrite normalised REE patterns are slightly LREE enriched with $La/Sm_N = 1.2$–1.4. Unusual spikes in Gd and Er in analysis CKB 89-13 MI 4 and MI 14 are regarded as analytical artefacts. In general, the melt inclusions display a relative restricted compositional variation this suggest that the inclusions were trapped from a magma reservoir which was homogeneous on a local scale and which was not evolving significantly on the time scale represented by the inclusion.

Discussion

Origin of troctolite blocks and links to Skaergaard cumulates

Figure 6 compares the compositions of plagioclase and olivine from the Skaergaard intrusion and blocks of the Campsite Dyke. The most primitive olivine composition in the Skaergaard intrusion is found in picrite blocks of the MBS. However, Kays and McBirney (1982) concluded that these picrites were more likely to be xenoliths of ultramafic rock from the Archean sequence than autoliths belonging to the intrusion. The Skaergaard olivine compositions are less magnesian than Fo_{74} (Hoover 1989b). In comparison, the blocks (Fo_{77-78}) and the chill (Fo_{80}) are rather more magnesian, but in terms of olivine composition the

troctolite blocks overlap with experimental data for Skaergaard (Thy et al. 2006; Toplis and Carroll 1995). The most primitive plagioclase compositions observed in the Skaergaard come from the perpendicular feldspar rock of the MBS with An_{77} (Hoover 1989b; Wager and Brown 1968) and MBS cumulates with $\sim An_{74}$ (Hoover 1989b). Wager and Brown (1968) suggested that the first cumulates crystallised plagioclase An_{77} whereas the most primitive analysed plagioclase composition in HZ is An_{73} (Humphreys 2009). Plagioclase in both the troctolitic blocks and the Campsite Dyke chill have higher anorthite content than Skaergaard cumulates and plot on an extension of the Skaergaard trend in Fig. 6. The troctolite blocks could therefore represent primitive HZ Skaergaard cumulates as proposed by Brooks and Nielsen (1990). Irvine et al. (1998) reached the same conclusion, but additionally suggested the alternative interpretation; that the blocks could represent a cumulate facies of the plagioclase ultraphyric dyke. The troctolitic blocks described here contain large plates of clinopyroxene oikocrysts optically enclosing plagioclase and olivine so texturally the pyroxene would not be regarded as a cumulus phase. HZ cumulates have plagioclase and olivine as co-precipitating liquidus (Irvine et al. 1998; references therein), hence, the cumulus assemblage of plagioclase and olivine in the blocks is therefore consistent with an origin from the HZ whereas the lack of cumulus olivine in the plagioclase ultraphyric dyke makes it unlikely that the blocks originate from this dyke.

The compositions of plagioclase (An_{79-82}), olivine (Fo_{80}) and Ca-rich pyroxene (Mg# 81) in the troctolite blocks are similar to the microphenocrysts in the outer member of the Campsite Dyke (An_{81}, Fo_{81}, Cpx Mg# $\sim$80) (Table 3; Fig. 6). Further, the major element compositions of melt inclusions in troctolite blocks are similar to the margins of the outer member of Campsite Dyke (Tables 1, 4), deviating only slightly in MgO and Na_2O and have comparable trace element concentrations (Fig. 5). This could support that the troctolite blocks could be autoliths from a plutonic facies of the Campsite Dyke and not HZ cumulates. If so, the blocks and the Campsite Dyke would probably be regarded as a Skaergaard like dyke like the most primitive FG-1 dykes.

A exploratory drill hole into the unexposed part of the intrusion unfortunately did not reveal the thickness of the HZ or the nature of the very first cumulates as it only extended about 150 m into the HZ (Humphreys 2009; Maaløe 1976), but it has been argued that the bottom of the drill hole is close to the intrusion base (Holness et al. 2007; Humphreys 2009). However, Nielsen (2004) models the HZ with an increasing thickness toward the south and the compositions of HZ gabbros or troctolites under the central and southern parts of the intrusion are not constrained.

Table 3 Average electron microprobe compositions of plagioclase, olivine and augite

	Plagioclase — Dykes								Plagioclase — Blocks		Olivine				Augite				
Type	Chill CD	Central CD	Central CD	Central CD^R	PUD	PUD	PUD^R	Troc	Troc	Troc	Chill CD	Chill CD	Troc	Troc	Chill CD	Chill CD	CD	PUD	Troc
Sample #	CKB 03-1	CKB 81-105	CKB 81-105	CKB 84-406	CKB 03-3	CKB 03-3	CKB 03-3	CKB 89-13	CKB 03-4	MM 30008C	MM 30008D	CKB 03-1	CKB 89-13	CKB 03-4	MM 30008D	CKB 03-1	CKB 81-105	CKB 03-3	CKB 89-13
n	12	12	18	15	15	12	10	12	15	10	12	8	9	12	5	6	15	12	18
SiO_2	47.80	49.57	55.68	56.27	49.03	53.84	59.44	47.13	47.89	47.16	41.71	40.05	39.51	39.61	51.1	51.69	52.08	50.75	51.61
TiO_2															0.75	0.78	0.78	1.53	0.72
Al_2O_3	32.61	31.86	27.40	26.57	32.05	28.59	24.18	32.95	33.19	31.99					3.39	3.35	2.56	3.00	2.98
Cr_2O_3																0.54	0.35	0.23	0.54
FeO^T	0.64	0.61	0.67	0.28	0.60	0.45	0.47	0.69	0.66	0.56	15.81	18.62	19.96	20.84	7.34	6.56	8.30	8.78	6.29
MnO											0.20	0.26	0.28	0.29	0.09	0.14	0.19	0.19	0.15
NiO												0.20	0.17	0.15					
MgO											41.75	40.52	40.49	40.31	16.06	15.45	15.35	14.46	15.56
CaO	16.52	15.17	9.18	8.81	15.46	11.49	6.38	16.76	16.51	16.91	0.24	0.34	0.34	0.34	22.20	21.34	20.14	20.19	21.07
Na_2O	2.17	2.82	6.12	6.38	2.68	4.83	7.44	1.97	2.05	2.38					0.17	0.27	0.27	0.36	0.26
K_2O	0.05	0.12	0.41	0.48	0.10	0.26	0.55	0.04	0.06	0.06									
Sum	99.79	100.15	99.45	98.79	99.91	99.46	98.46	99.54	100.36	99.06	99.71	99.99	100.75	101.53	101.10	100.11	100.01	99.48	99.18
Formula based on	8 Oxygen atoms								8 Oxygen atoms		4 Oxygen atoms				6 Oxygen atoms				
Si	2.203	2.266	2.525	2.562	2.248	2.451	2.695	2.180	2.193	2.196	1.047	1.022	1.008	1.006	1.876	1.904	1.928	1.898	1.916
Ti															0.021	0.022	0.022	0.043	0.020
Al	1.771	1.716	1.465	1.426	1.732	1.534	1.292	1.796	1.791	1.756					0.147	0.145	0.112	0.132	0.130
Cr																0.016	0.010	0.007	0.016
Fe	0.025	0.023	0.025	0.011	0.023	0.017	0.018	0.027	0.025	0.022	0.332	0.397	0.426	0.443	0.225	0.202	0.257	0.275	0.195
Mn											0.004	0.006	0.006	0.006	0.003	0.004	0.006	0.006	0.005
Ni											0.000	0.010	0.009	0.007					
Mg											1.563	1.541	1.540	1.527	0.879	0.848	0.847	0.806	0.861
Ca	0.816	0.743	0.446	0.430	0.759	0.560	0.310	0.830	0.810	0.844	0.006	0.009	0.009	0.009	0.873	0.842	0.799	0.809	0.838
Na	0.194	0.250	0.538	0.563	0.239	0.426	0.654	0.177	0.182	0.215					0.012	0.019	0.019	0.026	0.019
K																			
Total	5.007	4.998	5.000	4.992	5.002	4.988	4.970	5.009	5.001	5.032	2.953	2.984	2.997	2.998	4.036	4.003	3.999	4.002	4.000
Mg#											82.4	79.4	78.2	77.4	79.5	80.6	76.6	74.5	81.4
An%	80.6	74.3	44.3	42.1	75.7	55.9	31.1	82.3	81.3	79.4									

All oxides in weight %

Blank spaces not analysed, n is number of analyses that has been averaged

$Mg\# = 100 \times Mg/(Mg + Fe)$, $An\% = 100 \times Ca/(Ca + Na)$

Chill CD = chill of Campsite Dyke (outer member), central CD = Campsite Dyke (central member), PUD = plagioclase ultraphyric dyke, Troc = troctolite, ^{R} = rim compositions

Table 4 Major and trace element compositions of melt inclusions hosted in plagioclase in troctolite and suggested parental Skaergaard magmas

Label	CKB89-13MI4	CKB89-13MI5	CKB89-13MI6	CKB89-13MI7	CKB89-13MI8	CKB89-13MI9	CKB89-13MI10	CKB89-13MI11	CKB89-13MI13	CKB89-13MI14	CKB89-13MI18	CKB89-13MI23	CKB89-13MI31	Av*	SD	E.G 4507	KT-39	SK-TFDN	Bulk Av.
SiO_2	47.99	47.93	48.41	47.99	48.69	47.96	48.23	48.64	47.77	49.01	47.43	47.80	47.92	48.82	0.44	48.50	50.46	47.91	46.26
TiO_2	2.30	2.72	1.92	2.09	2.21	2.19	2.51	2.08	2.11	2.42	2.09	2.07	1.98	2.24	0.23	1.18	2.7	3.09	4.22
Al_2O_3	14.69	13.76	14.30	13.40	13.78	14.27	14.31	14.01	14.92	13.75	14.14	14.90	14.59	14.42	0.47	17.40	13.41	13.80	12.40
FeO_T	12.12	12.42	11.68	11.87	11.84	12.20	12.27	11.63	12.04	11.11	14.05	11.53	10.66	12.13	0.79	9.73	12.96	15.43	17.26
MgO	5.58	6.80	5.59	6.21	5.99	6.10	6.45	5.72	5.90	5.92	5.95	5.89	5.60	6.06	0.35	8.71	6.71	6.13	6.29
MnO	0.17	0.10	0.11	0.25	0.17	0.21	0.17	0.20	0.10	0.20	0.30	0.21	0.13	0.18	0.06	0.16	0.22	0.24	0.27
CaO	11.47	11.39	12.28	14.05	13.09	12.22	11.44	13.00	12.20	13.64	11.95	12.00	12.36	12.57	0.83	11.50	10.34	10.16	10.07
K_2O	0.33	0.41	0.66	0.21	0.26	0.44	0.48	0.25	0.53	0.21	0.38	0.51	0.22	0.38	0.15	0.25	0.57	0.40	0.36
Na_2O	3.33	3.12	3.30	2.23	2.44	2.93	2.96	2.80	2.59	3.04	2.75	2.49	4.66	3.01	0.61	2.39	2.41	2.57	2.40
P_2O_5	0.18	0.17	0.16	0.19	0.17	0.19	0.22	0.25	0.18	0.22	0.18	0.24	0.16	0.20	0.03	0.10	0.22	0.28	0.45
Sum	97.98	98.67	98.26	98.31	98.49	98.54	98.95	98.34	98.18	99.32	99.06	97.44	98.16						
Mg#	48.5	52.9	49.5	51.7	50.9	50.6	51.8	50.2	50.1	52.2	46.5	51.2	51.8		0.48	64.7	51.5	44.9	42.7
Fo#	73	77	74	76	75	75	76	75	75	76	72	75	76		1.31				
Mg# Cpx	78	81	79	80	80	80	80	79	79	81	77	80	80		1.14				
An%	73	74	74	83	81	76	75	78	78	78	77	79	67		3.96				
V	381		333	341	383		326		355	412		325		357	32				
Sr	262		354	343	373		307		319	400		325		335	42		214	241	
Y	28.5		22.6	23.4	25.2		30.9		27.8	30.5		24.3		26.7	3.2		27		
Zr	185		113	121	129		148		156	156		117		141	25	93	173	128	
Nb	14.6		8.5	9.4	10.4		11.8		12.5	15.4		8.8		11.4	2.6		16		
Ba	56		56	48	53		60		51	73		56		57	7.4	48	96	77	
La	13.30		9.38	10.04	11.06		14.28		12.23	13.63		9.76		11.71	1.9	5.6	12.14	10.67	
Ce	35.59		24.39	25.55	29.18		38.91		31.78	35.93		26.27		31.0	5.4	12.1	30.7		
Pr	5.15		3.53	3.73	4.09		5.43		4.55	4.95		3.88		4.4	0.7				
Nd	24.88		17.40	17.92	18.60		23.95		22.13	23.43		17.61		20.7	3.2	9.2	21.2		
Sm	6.52		4.38	4.94	4.54		6.47		5.64	6.82		5.27		5.57	0.9	2.5	5.78	5.07	
Eu	1.82		1.71	1.74	1.74		1.66		1.74	1.95		1.65		1.75	0.1	1.0	1.63		
Gd	4.91		4.61	4.13	4.57		6.84		5.89	6.25		5.03		5.28	0.8				
Dy	5.67		4.26	4.63	4.56		5.69		4.97	6.20		4.73		5.09	0.7				
Er	2.94		2.32	1.89	2.23		3.17		2.65	3.28		2.49		2.62	0.4				
Yb	2.31		1.84	1.89	1.76		2.77		2.33	2.57		2.02		2.18	0.4		2.39		

Major elements in weight % trace elements in μg/g

Blank spaces not analysed

* Average recalculated to 100%, SD: one standard deviation. EG4507 from Haskin and Haskin (1969) and McBirney (1996) KT-39 from Hoover (1989a) and McBirney (1996), SK-TFDN from Nielsen (2004) and Bulk Av. is from Ariskin (2002). Fo# calculated based on $K_D^{Fe–Mg} = 0.3$ (Roeder and Emslie 1970) Mg# for clinopyroxene based on $K_D^{Fe–Mg} = 0.23$ (Grove and Bryan 1983; Toplis and Carroll 1995) An% based on $K_D^{Na–Ca} = 1.4$ (Thy et al. 2006)
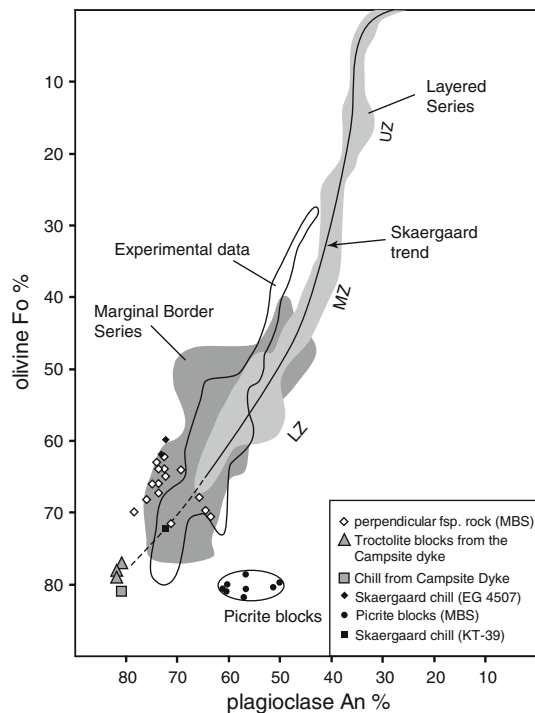
Fig. 6 Plot of olivine (mol% Fo) versus plagioclase (mol An%) for rocks in the Skaergaard intrusion, chilled Skaergaard rocks and samples from the present study. Light shaded area is composition of Layered Series cumulates from Thy et al. (in preparation) and McBirney (1996) plotted as a reference with the Skaergaard trend as a solid line from Wager and Brown (1968). The *darker shaded area* represents compositions in MBS from the Banded Division Rocks and Tranquil Division from Hoover (1989b). Perpendicular feldspar rocks from Hoover (1989b) and picrite blocks from Kays and McBirney (1982). Skaergaard chills E.G. 4507 from Wager (1960) and KT-39 from Hoover (1989a). Olivine, however, is not present in KT-39 but is taken from crystallisation experiments on a KT-39 sample (Hoover 1989a)

Are the melt inclusions in equilibrium with the host rock?

When interpreting melt inclusion data, it is always critical to assess whether the data represent true melt compositions. Below we address this in two ways; first, by evaluating the extent of compositional control by host plagioclase and second, calculating mineral compositions in equilibrium with the melt inclusions based on experimentally determined mineral melt equilibria.

A common problem with melt inclusions is to account for host wall crystallisation. Ideally, homogenisation will re-dissolve exactly this plagioclase part into the melt inclusion. However, over- or under-heating will result in flawed compositions. The studied melt inclusions were heated to 1,185°C and provide a minimum crystallisation temperature for the host plagioclase (Roedder 1984). The emplacement temperature of the parent Skaergaard magma has been estimated to 1,165–1,175°C based on phase
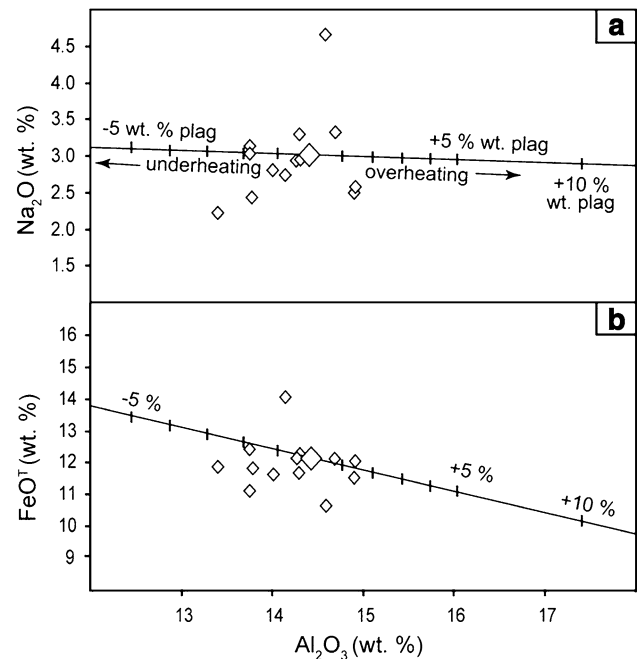
Fig. 7 Element plots for melt inclusions showing possible effect of plagioclase control. **a** Al_2O_3 versus Na_2O; **b** Al_2O_3 versus FeO^T. Small diamonds are analyses of individual melt inclusions and the large diamonds represent the average composition for the melt inclusions. Control line plotted between the average composition of the melt inclusions and the cumulus plagioclase hosting the melt inclusions (Table 3)

equilibria (Andersen 2006; Ariskin 2002) and partial melting experiments on LZa cumulates (Hoover 1978, 1989b; McBirney and Naslund 1990). Thy et al. (2009a) used a plagioclase thermometer to estimate the temperature of the initial magma to 1,150–1,160°C. The thermometer of Thy et al. (2009a) results in liquidus temperatures of 1,183–1,194°C for plagioclase in the troctolite blocks, matching perfectly the measured trapping temperature of the melt inclusions (1,185°C). To check potential plagioclase control we have plotted Na_2O (included in plagioclase) and FeO (excluded in plagioclase) versus Al_2O_3 (included in plagioclase) for the melt inclusions (Fig. 7). This analysis demonstrates that plagioclase control is <5% and therefore does not significantly influence the melt inclusion compositions. Based upon this we conclude that the compositional variations between individual melt inclusions are a primary feature.

The compositions of olivine and Ca-rich pyroxene in equilibrium with the melt inclusions have been calculated assuming a Fe_2O_3/FeO ratio of 0.15 in the melt (Brooks 1976) and Fe–Mg exchange distribution coefficients K_D^{Fe-Mg} [$(X_{FeO}/X_{MgO})^{crystal}/(X_{FeO}/X_{MgO})^{liquid}$ in moles] of 0.30 and 0.23, respectively (Grove and Bryan 1983; Roeder and Emslie, 1970; Thy et al. 2006; Toplis and Carroll, 1995). The calculated olivine compositions ranges from Fo_{72} to Fo_{77} and Mg# of Ca-rich pyroxene from 77 to 81

(Table 4). These compositions are close to olivine (Fo_{78}) and Ca-rich pyroxene (Mg# 81) in the troctolite blocks (Table 3). The composition of equilibrium plagioclase is more difficult to constrain because the K_D^{Na-Ca} defined as $(X_{NaO}/X_{CaO})^{plagioclase}/(X_{NaO}/X_{CaO})^{liquid}$ in moles varies depending on pressure and magma composition, and in particular on the volatile contents (Feig et al. 2006; Grove and Baker 1984; Grove and Bryan 1983; Panjasawatwong et al. 1995). Experimental data calculated for Skaergaard range from K_D^{Na-Ca} 1.1 (Toplis and Carroll 1995) to 1.4 (Thy et al. 2006). The melt inclusions are characterised by large variation in Na/Ca ratio (0.29–0.68) resulting in a considerable range for the calculated An %. Using a K_D^{Na-Ca} of 1.4 the calculated equilibrium plagioclase compositions ranges from An_{67} to An_{83} for the melt inclusions with an average of $An_{76 \pm 4}$. This is slightly lower than An_{79-82} measured in host plagioclase (Table 3) but still comparable and within error.

Cottrell et al. (2002) also discussed the potential role of diffusional equilibration between melt inclusions and host plagioclase resulting in modification of REE abundances in plagioclase-hosted melt inclusions. Plagioclase-hosted inclusions from this study have Eu and Sr contents that appear less variable than other trace elements of similar incompatibility (Fig. 5b; Cottrell et al. 2002; Kent 2008). Differences in variability of more compatible elements is one possible indication of diffusional equilibration (Cottrell et al. 2002), but could also reflect the effects of re-addition of plagioclase during re-homogenization. Overall we note that REE contents in melt inclusions overlap those of the host dykes, and importantly also appear to match the composition of specific East Greenland flood basalt sequences (see below). From this we argue that if post entrapment modification of REE contents in plagioclase-hosted melt inclusions did occur it was probably of relatively limited extent and resulted in little overall change in REE contents relative to analytical uncertainties.

Melt inclusions: parental magma of the Skaergaard intrusion?

In order to test if the inclusions could be a possible parental Skaergaard magma, we simulate fractional crystallisation of the melt inclusions using the COMAGMAT algorithm (Ariskin 2002; Ariskin et al. 1993) The latest version (3.65) of the software is optimised for ferrobasaltic systems in the temperature range 1,050–1,200°C (Ariskin 2002) and the simulation has been run at 1.5 kbar (Larsen and Tegner 2006) at the QFM buffer (Frost and Lindsley 1992; Lindsley et al. 1969; Sato and Valenza 1980; Thy et al. 2006, 2009b) based on a water-free assemblage. The results of the COMAGMAT simulation (Fig. 8) show that the average melt inclusion crystallises first plagioclase (An_{69} at
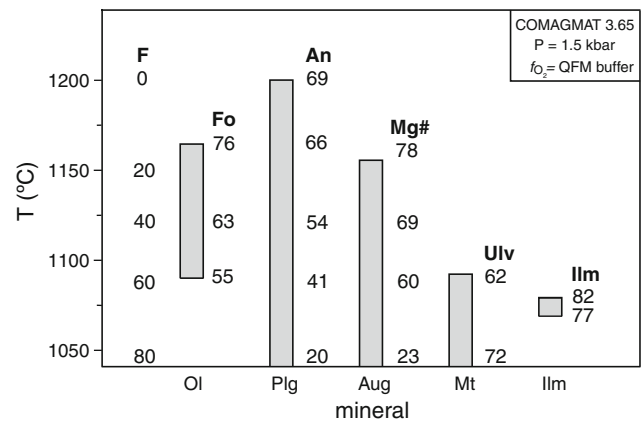

Fig. 8 Mineral compositions modelled with COMAGMAT (Ariskin et al. 1993) for the average composition of plagioclase hosted melt inclusions. Values to the right of magnetite and ilmente represent the percent of ulvöspinel and ilmentite component in solid solutions calculated using the equations of Stormer (1983). See text for details

1,198°C), then olivine (Fo_{78} at 1,165°C), then augite (Mg# 78 at 1,156°C) and finally Fe–Ti oxides (1,092°C). Plagioclase as the first mineral crystallising is in agreement with experimental findings in the Skaergaard marginal gabbros (Hoover 1989a) and experimental work on the FG-1 dykes with similar Mg# (Thy et al. 2006). However, we note that there is a long interval of plagioclase as the only crystallising phase and no pigeonite in the crystallising assemblage. The latter observation is, however, inconsistent with experimental data (Thy et al. 2006; Toplis and Carroll 1995) and with the results from a similar COMAGMAT simulation on a Skaergaard chill (Ariskin 1999) and with the Skaergaard paragenesis. The calculated An content An_{69} is also lower than that observed in the host plagioclase ($\sim An_{80}$). Nevertheless, the COMAGMAT modelling provides a reasonably close match to the cumulus assemblage and the composition of the most primitive cumulates observed in Skaergaard and the studies melt inclusions could represent early Skaergaard melt compositions.

The nature of the parental Skaergaard liquid has been the subject of considerable debate. So far three main approaches have been used to constrain the parental Skaergaard liquid; (1) chilled margins (2) bulk mass summation and (3) the FG-1 dykes (described above). (1) Chilled margins were used by Wager (1960) and Hoover (1978, 1989a, b) to constrain the parental magma. The initial liquid composition EG4507 sampled by Wager (1960) at the South–Western contact (Fig. 1a) has an olivine tholeiitic composition with Mg# 65, which is relatively primitive compared to melt inclusions in this study as well as other estimates (Fig. 9). KT-39 collected by Hoover (1989a) from the western margin (Fig. 1a) is characterised by a relatively high SiO_2 content

Fig. 9 Element plots of melt inclusions from blocks in the Campsite Dyke, FG-1 dykes A and C, and other previous estimates of Skaergaard parental liquid. Uncertainty bars for melt inclusion average are ±1 s. East Greenland Plateau Lavas subdivided into the Milne Land-, Geikie Plateau-, Skrænterne- and Rømer Fjord formations (Andreasen et al. 2004; Peate and Stecher 2003; Tegner et al. 1998b) are shown for comparison
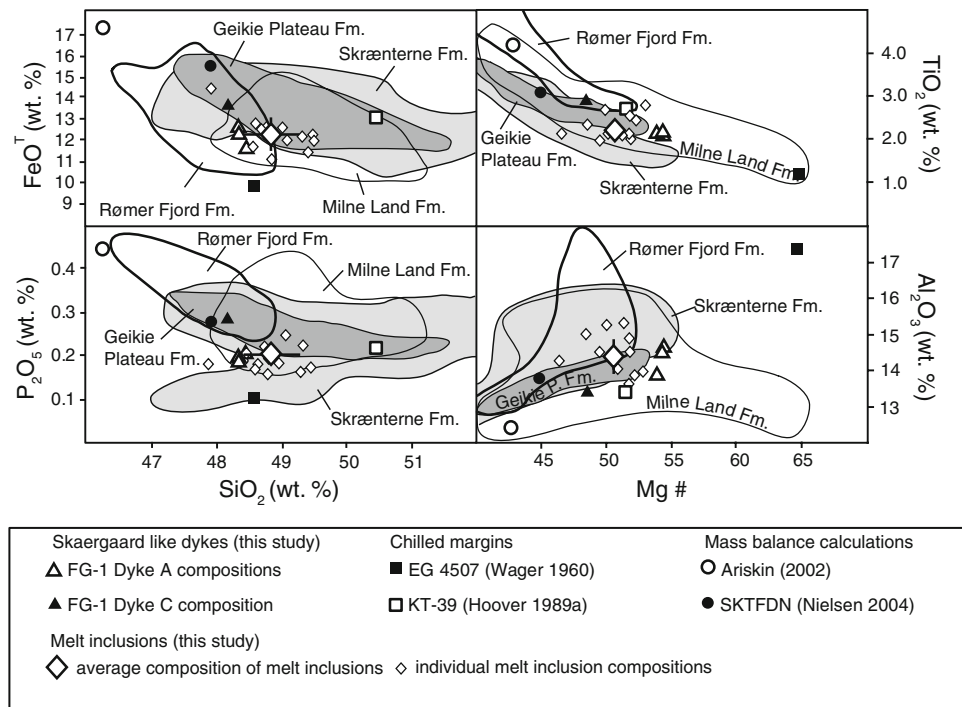
(50.5 wt.%). The chill shows some similarities with the melt inclusions such as comparable Mg#, FeO/TiO$_2$ (e.g. ~5) and good correlation for the trace elements with the exception of Sr (Table 4), but has somewhat lower Al$_2$O$_3$, CaO and Na$_2$O and higher FeO^T, TiO$_2$ and K$_2$O than the melt inclusions. (2) Ariskin (2002) and Nielsen (2004) calculated the bulk composition of Skaergaard by estimating the volume of the intrusion and its lithological sub-zones based on structural evidence and/or exploration drill core data, combined with average rock compositions of McBirney (1989). The composition SK-TFDN, proposed by Nielsen (2004) is a rather evolved (Mg# 45) ferrobasalt (Fig. 9) similar to high titanium East Greenland plateau lavas of the Geikie Formation, likewise the composition proposed by Ariskin (2002) is more evolved than other proposed Skaergaard magmas. Both mass-balance calculations estimate higher FeO^T, TiO$_2$ contents than the other methods possibly due to underestimation of the mass proportion of early plagioclase rich cumulates in the unexposed parts of the intrusion.

Figure 9 illustrates that the melt inclusions are well within the compositional range of previous Skaergaard estimates and the coeval flood basalts. The various suggested parental Skaergaard liquids appear to represent different magmas unrelated by fractional crystallisation as no correlation is observed between MgO and incompatible elements (K$_2$O, P$_2$O$_5$). The melt inclusions correlates most closely with the primitive compositions of the FG-1 dykes (comp. A) whereas the composition EG4507 (Wager 1960) is too enriched in Al$_2$O$_3$, depleted in FeO^T and trace

element concentrations (Table 4) compared to the melt inclusions and other proposed compositions to make it a likely early Skaergaard liquid. Similarly, the extreme FeO, P$_2$O$_5$ and low SiO$_2$ for the composition suggested by Ariskin (2002) precludes it as a good candidate for parental Skaergaard magma. It is difficult to demonstrate that the melt inclusions provide a better estimate of the parental Skaergaard magma than previous estimates, however, bulk mass summations depends strongly on assumptions of volumes and compositions. Chills samples are prone to contamination by the adjacent country rocks, and the relatively high SiO$_2$ and K$_2$O of KT-39 could be a result of contamination with granitic melt caused by thermal erosion along the contacts (Nielsen 2004). Furthermore, the variability of chill samples throws doubt on the validity of any compositional exercise based on this approach.

Linking Skaergaard to the flood basalt succession

The Skaergaard intrusion and the FG-1 dykes were emplaced contemporaneously with the East Greenland flood basalts and their petrogenesis is likely to be linked. The lava succession is divided into the Lower Lavas and the overlying Plateau Lavas (Fig. 10a). The Lower Lavas make up a 1.5–2 km thick volcanic succession emplaced locally into sedimentary basins in the Kangerlussuaq area (Fram and Lesher 1997; Hansen and Nielsen 1999; Nielsen and Brooks 1981; Utkins-Peate et al. 2003). The Lower Lavas are intruded by the Skaergaard intrusion (Fig. 10b) and are therefore older and petrogenetically unrelated to the
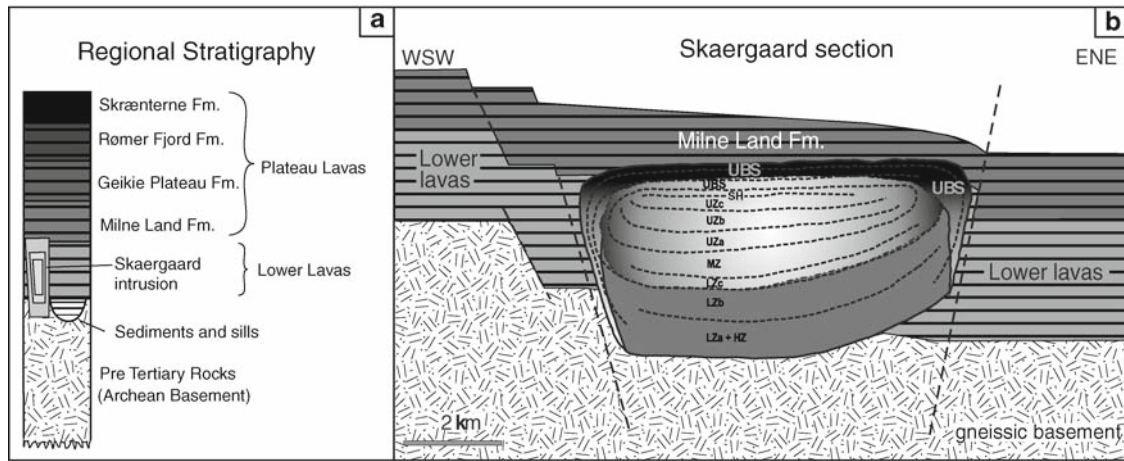
Fig. 10 a Simplified stratigraphic regional section of the East Greenland flood basalt succession. **b** Model section of the Skaergaard intrusion (modified from Larsen and Tegner 2006). *SH* Sandwich Horizon. Other abbreviations as in Fig. 1. See text for further explanation

intrusion. The overlying Plateau Lavas make up a true flood basalt succession that comprises more than 300 flows with a total thickness in excess of 5.5 km in the coastal area that erupted regionally over more than 60.000 km^2 (Nielsen and Brooks 1981; Pedersen et al. 1997). On the basis of flow morphology, petrography, and composition, the Plateau Lavas have been subdivided from base to top into: the Milne Land Formation, the Geikie Plateau Formation, the Rømer Fjord Formation and the Skrænterne Formation (Fig. 10a) (Larsen et al. 1989; Tegner et al. 1998b).

Previous studies have linked the Skaergaard intrusion to the Geikie Plateau Formation. Andreasen et al. (2004) showed rather restricted major element compositions in successive flows in the Geikie Plateau Formation with two major fractionation cycles and argued that the Skaergaard parental magma was a relatively evolved ferrobasalt similar to the most fractionated lavas in the these cycles. Nielsen (2004) also argued that the preferred parental magma obtained by bulk-summation is similar to lavas of the Geikie Plateau Formation. In contrast, the compositions obtained here for the melt inclusions in plagioclase of the troctolite blocks do not match the Geikie Plateau Formation (Fig. 11). Compared to the Geikie Plateau Formation, the melt inclusions have distinct Ce/Nb ratios at a given FeO^T indicating a link to the Milne land Formation (Fig. 11a). The average composition of the melt inclusions fall outside or barely overlap with the major element plots of the Geikie Plateau Formation whereas the average composition of the melt inclusions is well within the compositional range of the Milne Land Formation (Fig. 9). Also, the ratio of the middle- to heavy-rare earth elements, expressed by Dy/Yb$_N$, is higher in the melt inclusions relative to the Geikie Plateau Formation (Fig. 11b). Tegner et al. (1998b) showed that there is a distinct up-section
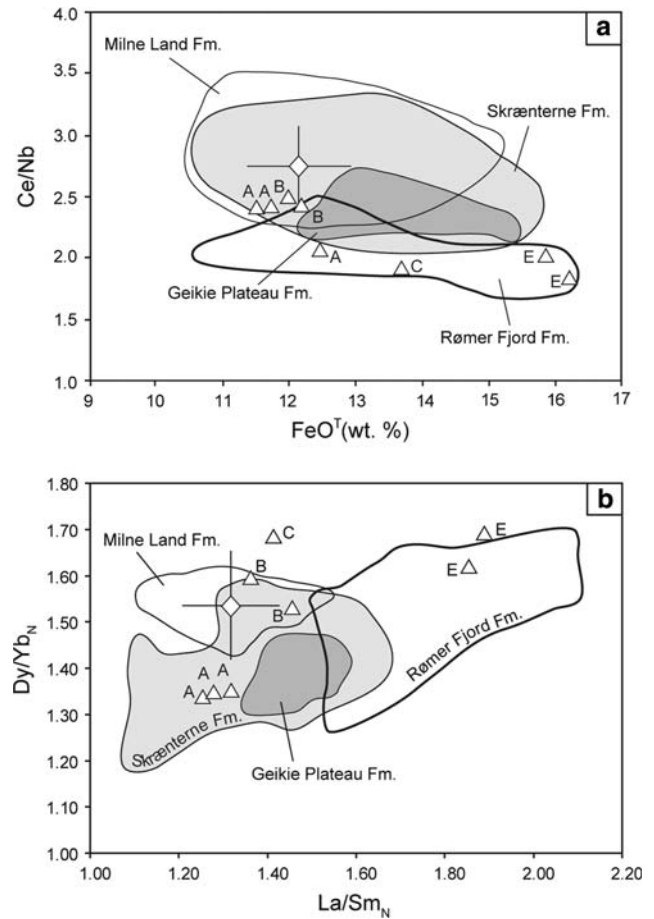

Fig. 11 a Major- and trace element variations for the average melt inclusion composition in the Campsite Dyke (*diamonds*) and FG-1 dykes (*triangles*) from this study. Uncertainty bars for melt inclusion averages are ±1 s. **a** Ce/Nb versus FeO^T, **b** La/Sm$_N$ versus Dy/Yb$_N$ where subscript N denotes chondrite normalised ratios. For comparison are shown the Plateau Lavas, Plateau lavas data from Andreasen et al. (2004) and Tegner et al. (1998b)

decrease in Dy/Yb_N through the Milne Land and Geikie Plateau Formations and linked this to a secular decrease in the depth of melting. The Dy/Yb_N of the melt inclusions falls in the middle of the field defined by the lavas of the Milne Land Formation and does not overlap with the Geikie Plateau Formation (Fig. 11b). Considering this we conclude that the major and trace element compositions of the melt inclusions are similar to the lavas of the Milne Land Formation and certainly different from those of the Geikie Plateau Formation. Based on the compositions alone, we cannot rule out a linkage to the upper Rømer Fjord and Skrænterne Formations, but such a link is not tenable given the constraints on the depth of emplacement discussed below.

The depth of emplacement of the Skaergaard intrusion has been debated. Lindsley et al. (1969) and Hirschmann et al. (1997) have argued, based on the coexistence of tridymite and ferrobustamite, that the Sandwich Horizon formed at a pressure of 0.6 ± 0.1 kbar, corresponding to an overburden of less than 2 km. The UBS that structurally overlies the Sandwich Horizon (Fig. 10b), is ~ 900 m thick (Naslund 1984) at the margins of the intrusion and according to Nielsen (2004) likely on average 600 m stratigraphic height, which implies that the lava cover over the intrusion was no more than 1.1–1.4 km thick. Recently, Larsen and Tegner (2006) showed that fluid inclusions in quartz in granophyre pockets in LZa formed at a lithostatic pressure of 1.8 ± 0.5 kbar, corresponding to a pressure of 0.7 ± 0.5 kbar at the roof of the intrusion. Based on these findings Larsen and Tegner (2006) therefore argue that the emplacement of the Skaergaard intrusion was better linked to the eruption of the Milne Land Formation of the Plateau Lavas (Fig. 10b). Our data on the compositions of the melt inclusions in the troctolite blocks is consistent with this conclusion.

In contrast to the melt inclusions, the compositions of the FG-1 A to C dykes show considerable variation that overlap with several compositional fields for the Plateau Lava formations (Fig. 11). The C dyke is distinctly iron-rich (13.7 wt.% FeO^T) and low in Ce/Nb and compares only with the evolved fractionation cycles of the Rømer Fjord Formation (Fig. 11a). Also, the steep rare-earth element patterns with high La/Sm_N and Dy/Yb_N in the E dykes are similar only to the Rømer Fjord Formation (Fig. 11b). Therefore, we conclude that the FG-1 dykes represent magma types equivalent to the entire flood basalt succession.

Conclusions

Knowledge of the parental magma composition is mandatory for geochemical modelling of the Skaergaard intrusion. We have studied melt inclusions in plagioclase of troctolite blocks in the Campsite Dyke and the FG-1 dyke swarm to constrain the parental magma. No approach or individual rock sample is likely to provide a perfect match for the bulk composition of the intrusion. However, in contrast to previous approaches, using chilled marginal rocks, associated dykes, or mass-balance, melt inclusions are based on the analysis of true liquids. We conclude that:

1. The Campsite Dyke, exposed in the Home Bay area, contains blocks of several types. Troctolitic blocks contain Fo_{78} olivine and An_{82} plagioclase and are seen as possible primitive blocks from HZ as originally suggested by Brooks and Nielsen (1990).

2. Plagioclase phenocrysts in the troctolitic blocks contain crystallised, primary melt inclusions. Although trapped in a plutonic environment, the melt inclusions are microcrystalline and represent genuine melt compositions in equilibrium with the phenocryst assemblage of the host rock.

3. Major- and trace element composition of re-heated melt inclusions are slightly different from previous estimates of the parental magma to the Skaergaard intrusion. Their major and trace element compositions demonstrate a link to the Milne Land Formation, the lowermost regional flood basalt formation rather than the overlying Giekie Formation in agreement with findings by Larsen and Tegner (2006).

4. The FG-1 dykes, previously taken to illustrate the liquid line of descent of the Skaergaard intrusion (Brooks and Nielsen 1978, 1990), have a relatively large compositional variation that covers the entire range of the coeval flood basalt succession. These dykes are therefore re-interpreted as feeder dykes that were active throughout the main phase of flood basalt volcanism.

References

Andersen JCØ (2006) Postmagmatic sulphur loss in the Skaergaard intrusion: implications for the formation of the Platinova Reef. Lithos 92:198–221

Andreasen R, Peate DW, Brooks CK (2004) Magma plumbing systems in large igneous provinces: inferences from cyclical variations in Palaeogene East Greenland basalts. Contrib Mineral Petrol 147:438–452

Ariskin AA (1999) Phase equilibria modelling in igneous petrology. Use of COMAGMAT model for simulating fractionation of ferro-basaltic magmas and the genesis of high-alumina basalt. J Volcanol Geotherm Res 90:115–162

Ariskin AA (2002) Geochemical themometry of the layered series rocks of the Skaergaard intrusion. Petrology 10:495–518

Ariskin AA, Frenkel MY, Barmina GS (1993) COMAGMAT: a fortran program to model magma differentiation processes. Comput Geosci 19:1155–1170

Blank HR, Gettings ME (1973) Subsurface form and extent of the Skaergaard intrusion, East Greenland. EOS Trans Am Geophys Union 54:507

Brooks CK (1976) The Fe_2O_3/FeO ratio of basalt analyses: an appeal for a standardized procedure. Bull Geol Soc Denmark 25:117–120

Brooks CK, Gleadow AJW (1977) A fission-track age for the Skaergaard intrusion and the age of the East Greenland basalts. Geology 5:539–540

Brooks CK, Nielsen TFD (1978) Early Stages in the differentiation of the Skaergaard magma as revealed by a closely related suite of dike rocks. Lithos 11:1–14

Brooks CK, Nielsen TFD (1990) The differentiation of the Skaergaard intrusion. A discussion of R. H. Hunter and R. S. J. Sparks (Contrib Mineral Petrol 95:451–461). Contrib Mineral Petrol 104:244–247

Cottrell E, Spiegelman M, Langmuir CH (2002) Consequences of diffusive reequilibration for the interpretation of melt inclusions. Geochem Geophy Geosy 3. doi:000175371900001

Danyushevsky LV, McNeill AW, Sobolev AV (2002) Experimental and petrological studies of melt inclusions in phenocrysts from mantle-derived magmas: an overview of techniques, and complications. Chem Geol 183:5–24

Feig ST, Koepke J, Snow JE (2006) Effect of water on tholeiitic basalt phase equilibria: an experimental study under oxidizing conditions. Contrib Mineral Petrol 152:611–638

Fram MS, Lesher CE (1997) Polybaric differentiation of magmas of the East Greenland Early Tertiary flood basalt province. J Petrol 38:231–275

Frezzotti M-L (2001) Silicate-melt inclusions in magmatic rocks: applications to petrology. Lithos 55:273–299

Frost BR, Lindsley DH (1992) Equlibria among Fe–Ti oxides, pyroxenes, olivine, and quartz: Part II. Application. Am Mineral 77:1004–1020

Gleadow AJW, Brooks CK (1979) Fission track dating, thermal histories and tectonics of igneous intrusions in East Greenland. Contrib Mineral Petrol 71:45–60

Grove TL, Baker MB (1984) Phase equilibrium controls on the tholeittic versus calc-alkaline differentiation trends. J Geophys Res 89:3253–3274

Grove TL, Bryan WB (1983) Fractionation of pyroxene-phyric MORB at low pressure: an experimental study. Contrib Mineral Petrol 84:293–309

Hamilton MA, Brooks CK (2004) A precise U-Pb zircon age for the Skaergaard intrusion. In: 15th annual Goldschmidt conference. Geochim Cosmochim Acta, pp A587

Hanghøj K, Rosing M, Brooks CK (1995) Evolution of the Skærgaard magma: evidence from crystallized melt inclusions. Contrib Mineral Petrol 120:265–269

Hansen H, Nielsen TFD (1999) Crustal contamination in Palaeogene East Greenland flood basalts: plumbing system evolution during continental rifting. Chem Geol 157:89–118

Haskin LA, Haskin MA (1969) Rare-earth elements in the Skaergaard intrusion. Geochim Cosmochim Acta 32:433–447

Hirschmann MM, Renne PR, McBirney AR (1997) ^{40}Ar/^{39}Ar dating of the Skaergaard intrusion. Earth Planet Sci Lett 146:645–658

Holness MB, Nielsen TFD, Tegner C (2007) Textural maturity of cumulates: a record of chamber filling, cooling rate and large-scale convection in layered intrusions. J Petrol 48:141–157

Hoover JD (1978) Meltning relations of a new chilled margin sample from the Skaergaard intrusion. Carnegie Inst Wash Yearbook 77:739–743

Hoover JD (1989a) The chilled marginal gabbro and other contact rocks of the Skaergaard intrusion. J Petrol 30:441–477

Hoover JD (1989b) Petrology of the marginal border series of the Skaergaard intrusion. J Petrol 30:399–441

Humphreys MCS (2009) Chemical evolution of intercumulus liquid as recorded in plagioclase overgrowth rims from the Skaergaard intrusion. J Petrol 50:127–145

Irvine TN (1991) Emplacement of the Skaergaard Intrusion. Carnegie Inst Wash Yearbook 91:91–96

Irvine TN, Andersen JCØ, Brooks CK (1998) Included blocks (and blocks within blocks) in the Skaergaard intrusion: geologic relations and the origins of rhythmic modally graded layers. Geol Soc Am Bull 110:1398–1447

Jakobsen JK, Veksler IV, Tegner C, Brooks CK (2005) Immiscible iron- and silica-rich melt in basalt petrogenesis documented in the Skaergaard intrusion. Geology 33:885–888

Kays MA, McBirney AR (1982) Origin of the picrite blocks in the marginal border group of the Skaergaard intrusion, East Greenland. Geochim Cosmochim Acta 46:23–30

Kent AJR (2008) Melt inclusions in basaltic and associated volcanic rocks. In: Putirka KD, Tepley FJ (eds) Mineral, inclusions and volcanic processes. Rev Mineral Geochem 69:173–231

Kent AJR, Elliott TR (2002) Melt inclusions from Marianas arc lavas: implications for the composition and formation of island arc magmas. Chem Geol 183:263–286

Kent AJR, Baker JA, Wiedenbeck M (2002) Contamination and melt aggregation processes in continental flood basalts constraints from melt inclusions in Oligocene basalts from Yemen. Earth Planet Sci Lett 202:577–594

Kystol J, Larsen LM (1989) Analytical procedures in the Rock Geochemical Laboratory of the Geological Survey of Denmark and Greenland. Geol Greenland Surv Bull 184:59–62

Larsen RB, Tegner C (2006) Pressure conditions for the solidification of the Skaergaard intrusion: eruption of East Greenland flood basalts in less than 300,000 years. Lithos 92:181–197

Larsen LM, Watt WS, Watt M (1989) Geology and petrology of the Lower Tertiary plateau basalts of the Scoresby Sund region, East Greenland. Geol Greenland Surv Bull 157:1–164

Li CS, Ripley ME, Sarkar A, Shin DH, Maier WD (2005) Origin of phlogopite-orthopyroxene inclusions in chromites from Merensky Reef of the Bushveld Complex, South Africa. Contrib Mineral Petrol 150:119–130

Lindsley DH, Brown GM, Muir ID (1969) Conditions of the ferrowollastonite-ferrohedebergite inversion in the Skaergard intrusion, East Greenland. Mineral Soc Am Spec Pap 2:193–201

Maaløe S (1976) The zoned plagioclase of the Skaergaard intrusion, East Greenland. J Petrol 17:398–419

McBirney AR (1989) The Skaergaard Layered Series: I. Structure and average compositions. J Petrol 30:363–399

McBirney AR (1995) Mechanisms of differentiation in the Skaergaard intrusion. J Geol Soc Lond 152:421–435

McBirney AR (1996) The Skaergaard intrusion. In: Cawthorn RG (ed) Layered intrusions. Developments in petrology 15. Elsevier, Amsterdam

McBirney AR, Naslund HR (1990) The differentiation of the Skaergaard intrusion. A discussion of R.H. Hunter and R.S.J. Sparks (Contrib Mineral Petrol 95:451–461). Contrib Mineral Petrol 104:235–240

McDonough WF, Sun S-s (1995) The composition of the Earth. Chem Geol 120:223–253

Momme P, Wilson JR (2002) The Kraemer Island macrodyke, East Greenland: solidification of a flood basalt conduit. Geol Mag 139:171–190

Naslund HR (1984) Petrology of the Upper Border Series of the Skaergaard intrusion. J Petrol 25:185–212

Nielsen TFD (1978) The Tertiary dike swarms of the Kangerdlugssuaq area, East Greenland. An example of magmatic development during continental break-up. Contrib Mineral Petrol 67:63–78

Nielsen TFD (2004) The shape and volume of the Skaergaard intrusion, Greenland: implications for mass balance and bulk composition. J Petrol 45:507–530

Nielsen TFD, Brooks CK (1981) The East Greenland rifted continental margin. An examination of the coastal flexure. J Geol Soc Lond 138:559–568

Norton D, Taylor HP Jr, Bird DK (1984) The geometry and high-temperature brittle deformation of the Skaergaard intrusion. J Geophys Res 89:10178–10192

Panjasawatwong Y, Danyushevsky LV, Crawford AJ, Harris KL (1995) An experimental study of the effects of melt composition on plagioclase—melt equilibria at 5 and 10 kbar: implications for the origin of magmatic high-An plagioclase. Contrib Mineral Petrol 118:420–432

Peate DW, Stecher O (2003) Pb isotope evidence for contributions from different Iceland mantle components to Palaeogene East Greenland flood basalts. Lithos 67:39–52

Pedersen AK, Watt M, Watt WS, Larsen LM (1997) Structure and stratigraphy of the Early Tertiary basalts of the Blosseville Kyst, East Greenland. J Geol Soc Lond 154:565–570

Roedder E (1984) Fluid inclusions. In: Ribbe PH (ed) Rev Mineral 12

Roeder PL, Emslie RF (1970) Olivine-liquid equilibrium. Contrib Mineral Petrol 29:275–289

Sato M, Valenza M (1980) Oxygen fugacites of the layered series of the Skaergaard intrusion, East Greenland. Am J Sci 280-A:134–158

Sobolev AV, Shimizu N (1993) Ultra-depleted primary melt included in an olivine from the Mid-Atlantic Ridge. Nature 363:151–154

Spandler CJ, Eggins SM, Arculus RJ, Mavrogenes JA (2000) Using melt inclusions to determine parent-magma compositions of layered intrusions: application to the Greenhills Complex (New Zealand), a platinum group minerals-bearing, island-arc intrusion. Geology 28:991–994

Spandler C, Mavrogenes J, Arculus R (2005) Origin of chromitites in layered intrusions: evidence from chromite-hosted melt inclusions from the Stillwater Complex. Geology 33:893–897

Stormer JC Jr (1983) The effects of recalculations on estimates of temperature and oxygen fugacity from analyses of multicomponent iron-titanium oxides. Am Mineral 68:586–594

Tegner C, Duncan RA, Bernstein S, Brooks CK, Bird DK, Storey M (1998a) ^{40}Ar–^{39}Ar geochronology of Tertiary mafic intrusions along the East Greenland rifted margin: relation to flood basalts and the Iceland hotspot track. Earth Planet Sci Lett 156:75–88

Tegner C, Lesher CE, Larsen LM, Watt WS (1998b) Evidence from the rare-earth element record of mantle melting for cooling of the Tertiary Iceland plume. Nature 391:591–594

Thy P, Lesher CE, Nielsen TFD, Brooks CK (2006) Experimental constrains on the Skaergaard liquid line of descent. Lithos 92:154–180

Thy P, Lescher CE, Tegner CK (2009a) Liquidus temperatures of the Skaergaard magma. Am Mineral (revised manuscript submitted)

Thy P, Lescher CE, Tegner CK (2009b) The Skaergaard liquid line of descent revisited. Contrib Mineral Petrol 157:735–747

Toplis MJ, Carroll MR (1995) An experimental study of the influence of oxygen fugacity on Fe–Ti oxide stability, phase relations, and mineral-melt equilibria in ferro-basaltic systems. J Petrol 36:1137–1171

Utkins-Peate IU, Larsen M, Lesher CE (2003) The transition from sedimentation to flood volcanism in the Kangerlussuaq Basin, East Greenland. Basaltic pyroclastic voicanism during initial Palaeogene continental break-up. J Geol Soc Lond 160:759–772

Vincent EA (1953) Hornblende-lamprophyre dykes of basaltic parentage from the Skaergaard area, East Greenland. Q J Geol Soc Lond 109:21–51

Wager LR (1960) The major element variation of the Layered Series of the Skaergaard intrusion and a re-estimation of the average composition of the Hidden Layered Series and of the successive residual magmas. J Petrol 1:364–398

Wager LR, Brown GM (1968) Layered igneous rocks. Oliver and Boyd, Edinburgh

Wager LR, Deer WA (1939) Geological investigations in East Greenland, Part III. The petrology of the Skaergaard Intrusion, Kangerdlugssuaq, East Greenland. Medd Grønland 105:1–352